On the effect of the non-constant approach velocity on the liquid film drainage

Runci Song, Luchang Han*, Ling Zhang, Shangyu Tang

School of Chemical Engineering, Xiangtan University, Hunan 411105, China

Abstract: A coupling framework for modeling the non-constant-velocity approach of two fluid particles and the curved film drainage was developed, and an improved model was presented to predict the variable-velocity approach. Using this framework, the effect of the constant-velocity and variable-velocity approach on liquid film drainage was investigated. Two film drainage models based on immobile interface and fully mobile interface were adopted. The simulation results showed that the film thinning rate of the former is much less than that of the latter. In the case of constant-velocity approach, the immobile interface model showed a relatively flat curved film, while in the case of variable-velocity approach, three types of film, wimple, pimple and dimple, can be found. The different combinations of the drainage models and the approach velocity boundary conditions were compared with the experiments. The fully mobile interface model with variable-velocity approach can reasonably predict the coalescence and rebound of bubbles.

Keywords: bubble, approach, film drainage, coalescence, rebound

* Author to whom correspondence should be addressed: hanlc@xtu.edu.cn

1. INTRODUCTION

The coalescence phenomenon of fluid particles (bubbles or droplets) is often encountered in industrial equipment such as bubble column, stirred tank, distillation column etc. The coalescence usually plays an important role in determining mass transfer and heat transfer of multiphase system. Whether coalescence is beneficial to actual operation depends on the scene it is applied to. In the process of chemical reaction, larger contact area between phases is expected, while in foaming separation process, larger bubble volume is expected[1].Therefore, the detailed study on the coalescence process will be valuable to help people to adjust and control the fluid particle size or interphase contact area in multiphase flow.

Some investigations[1-6] used computational fluid dynamics (CFD) simulation (volume of fluid method, level-set method) to analyze the deformation, rupture and coalescence of fluid particles. Although the CFD simulation can describe the dynamics of droplets or bubbles, once the two fluid particles are in close contact, the simulation results are easy to show the non-physical characteristics, such as the numerical pseudo-coalescence of two bubbles[7]. The accuracy of numerical simulation is limited by the size of mesh, however, and the coalescence process between bubbles spans at least five orders of magnitude with respect to the liquid film thickness, which means that a very fine mesh setting is required to accurately describe the coalescence process. Although the current computing technology has been rapidly developed, it still consumes huge computing costs in the face of complex multiphase systems. Therefore, another more economical and effective phenomenological modeling method is still widely used. Based on different reasonable assumptions, researchers have built a large number of coalescence rate (or frequency) models[8-20]. Liao and Lucas[21] reviewed the early coalescence rate models in detail. Some interesting work on the application of coalescence rate models to different reactor simulations can also be found[16-17, 22-26].

In order to provide the coalescence time or critical coalescence velocity required in the coalescence rate model, a detailed study on the liquid film drainage process is

required. Some insightful reviews[7, 27]on the construction of film drainage model can be found. Virtually, the coalescence process of fluid particles is very complicated, and some reasonable assumptions are necessary. The coalescence process of two fluid particles driven by external force can be simply divided into three processes: fluid particles approach each other to form a liquid film, film is thinning and film ruptures. Since the time of liquid film rupture is very short compared with the time of approach process or liquid film drainage process, most studies focused on the first two processes. In terms of the research of approach process, based on the assumption of a planar film, Svendsen and Luo[28] performed a force balance analysis on two equal-sized or unequal-sized bubbles colliding along the direction of the center of mass. The equation of two bubbles approaching each other and the equation of motion of the mass center of two-bubble system were obtained. Hagesaether *et al*.[29] used the same method, but takes more account of ellipsoid fluid particles and lubrication forces in the model. Klaseboer *et al*.[30] analyzed the process of buoyancy driven bubble impacting horizontal solid interface, and considered the deformation of interface during bubble collision, and established a force balance model. Their model can predict the rebound process of bubble hitting solid interface.

On the other hand, according to whether the interface is deformable, the film drainage model can be divided into a planar film model[31-33]and a curved film model[34-37]. The assumption of the planar film model is that, in the process of liquid film thinning, the liquid film interface (or film surface) is always a pair of parallel plane. Although this type of model is simple and easy to calculate, it may only be suitable for fluid particles of smaller size (d<1mm). The assumption that the thickness of liquid film is uniform in radial direction implies that there is no pressure gradient in the radial direction. However, some experiments[38-40] have observed that there is a dimple on the interface of liquid film during the drainage process, which means that there must be an uneven distribution of pressure in the liquid film. Therefore, the planar film model may be too simplified to describe the physical process of real film drainage. Different from the planar film model, the curved film model takes into account the characteristics of the interface during the drainage and thinning process.

According to the mobility of the interface, it can be divided into a fully mobile interface model, a partially mobile interface model and an immobile interface model. Most models were based on the assumption that lubrication approximation and axisymmetric flow. The film drainage rate is controlled by the flow inside the fluid particle and the flow of continuous phase in the liquid film. Davis *et al*.[41] used the boundary integral method to study the flow in the droplet, and obtained the tangential velocity of the liquid film interface contributed by the droplet flow. When the tangential velocity of liquid film interface is 0, it is an immobile interface model, whereas on the contrary, it is a mobile model. The model of Davis *et al*.[41] has a significant disadvantage, that is, there are natural singularities in the boundary integral equation, which brings great difficulty to the calculation of the model. Nevertheless, their model has been applied by many researchers[36,37,42,43]. Klaseboer *et al*.[37] investigated the immobile model and the mobile model under constant velocity boundary conditions. Compared with the coalescence experiment of high viscosity droplets, they found that the former had better prediction ability, while the latter predicted a smaller order of magnitude of liquid film thickness. Bazhlekov *et al*.[36] introduced the viscosity ratio of two phases into the dimensionless equation of liquid film drainage, and connected the immobile model and partial mobile model by changing the viscosity ratio. However, their models still used the boundary condition of constant velocity or constant force. Abid and Chesters[42] investigated the film drainage and liquid film rupture between two droplets under the condition of constant approach velocity. They found that the drainage rate of liquid film under constant velocity boundary condition is significantly higher than that under constant force boundary condition. Recently, Ozan and Jakobsen[43] followed the work of Bazhlekov *et al*.[36] and Klaseboer *et al*.[37] to study the effect of approach velocity on the coalescence time of fluid particles, and found that, with the increase of the approach velocity, the coalescence time showed a non-monotonic trend of decreasing to a minimum value and then increasing. Although this conclusion was obtained at different constant approach velocity, it was enough to show that the boundary conditions have an important influence on the film drainage.

Most of film drainage models based on the lubrication approximation omitted the inertia term and time derivative term in the momentum equation for the liquid film flow, so the simplification is large. There is another less simplified model to be found. Chesters and Hofman[34] suggested that under low viscosity systems (such as water-air), the liquid film interface is fully mobile, and film drainage is determined by the flow of the continuous phase inside the liquid film. Starting from the continuity equation and momentum equation describing the liquid film flow, they constructed a more complete model of liquid film drainage and thinning. However, they used a boundary condition of constant approach velocity that is inconsistent with reality. In addition, because the model is less simplified, there are more nonlinear terms in the film drainage equation, which makes it difficult to be solved, so the model has not been widely promoted.

The drainage of liquid film in the process of fluid particle collision is determined by the boundary conditions provided by the flow field environment. However, to the best of our knowledge, in most of the deformable interface drainage models, either constant velocity boundary conditions or constant force boundary conditions are used. In practical cases, the flow field where the fluid particles are located usually has high disturbance. Correspondingly, the constant velocity or constant force boundary conditions may no longer be applicable. Therefore, it is necessary to study the influence of non-constant velocity boundary conditions on the liquid film drainage.

This paper will focus on the investigation of the influence of variable approach velocity boundary conditions on the liquid film drainage process. Our drainage models follow those of Chesters and Hofman[34] and Klaseboer *et al*.[37], for the fully mobile and immobile interfaces, respectively, with a constant or non-constant velocity boundary conditions. An improved version of Svendsen and Luo model[28] of approach of fluid particles is proposed to predict a time-dependent boundary condition. Considering the difficulty of solving the full mobile interface model (using uniform mesh is easy to cause the numerical oscillation and divergence in the late stage of drainage process), we use an effective adaptive moving mesh algorithm. The different combinations of the two drainage models and different boundary conditions are

compared with the head-on collision experiment of two bubbles. The characteristics of the two models under two different boundary conditions are explored. Finally, the simulation results are compared with the single event of two bubbles head-on collision recorded in the experiment.

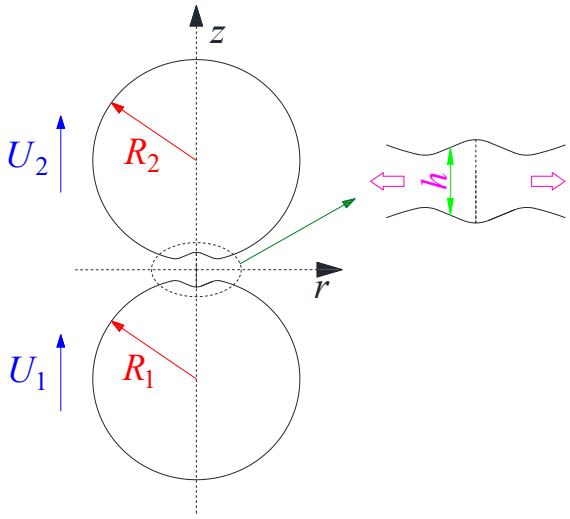

Fig. 1 Sketch of the approach and liquid film drainage processes of two fluid particles

2. MATHEMATICAL MODELS

As shown in Fig.1, two bubbles or droplets approach each other along the direction of the line between the center of mass, forming a liquid film between the two fluid particles. Liquid in the film is continuously squeezed out, and the film is thinning. The *r*-direction continuous flow in a liquid film in cylindrical coordinates can be described by mass conservation (Eq.(1)) and momentum conservation (Eq.(2)).

$$\frac{1}{r}\frac{\partial}{\partial r}(ru)+\frac{\partial u}{\partial z}=0 \tag{1}$$

$$\begin{aligned}&\rho_c\left(\frac{\partial u}{\partial t}+u\frac{\partial u}{\partial r}+\frac{w}{r}\frac{\partial u}{\partial \theta}-\frac{w^2}{r}+v\frac{\partial u}{\partial z}\right)\\&=-\frac{\partial P}{\partial r}+\mu_c\left[\frac{\partial}{\partial r}\left(\frac{1}{r}\frac{\partial}{\partial r}(ru)\right)+\frac{1}{r^2}\frac{\partial^2 u}{\partial \theta^2}-\frac{2}{r^2}\frac{\partial w}{\partial \theta}+\frac{\partial^2 u}{\partial z^2}\right]\end{aligned} \tag{2}$$

Where u, v, and w are the fluid flow velocities in the r, z, and θ directions in the liquid film, and μ_c and ρ_c are the continuous phase viscosity and density, respectively.

In order to obtain the film thickness thinning equation, some necessary assumptions often appear in the modeling of fluid particles coalescence, as follows:

(1) Isothermal, incompatible, pure Newtonian flow system (viscosity, density and surface tension are constant).

(2) The flow in the liquid film is approximately axisymmetric, and only the flow in the r direction is considered (the flow in the z and θ directions is not considered).

(3) Except for the liquid film region during the drainage, the fluid particles are considered to remain spherical ($r_f << h << R$).

(4) The pressure P inside the liquid film is independent of the axial direction (i.e. $\frac{\partial P}{\partial z} \approx 0$).

2.1 Fully mobile interface model

Chesters and Hofman[34] assumed that the pressure P and velocity u were evenly distributed in the z direction in the liquid film for the fully mobile film interface. In the cylindrical coordinate system, the relationship between the film thickness h and time t is obtained by the mass conservation in the liquid film as follows

$$\frac{\partial h}{\partial t} = -\left(\frac{hu}{r} + h\frac{\partial u}{\partial r} + u\frac{\partial h}{\partial r} \right) \tag{3}$$

Where, u is the drainage velocity at the radial position r of the film, which can be obtained by combining Eq.(2) with the above assumptions of (2) and (4) and fully mobile interface condition. That is,

$$\frac{\partial u}{\partial t} = -u\frac{\partial u}{\partial r} - \frac{1}{\rho_c}\frac{\partial P}{\partial r} + \frac{\mu_c}{\rho_c}\left[\frac{\partial}{\partial r}\left(\frac{1}{r}\frac{\partial}{\partial r}(ru) \right) + \frac{\partial^2 u}{\partial z^2} \right] \tag{4}$$

The first to third terms on the right hand side of Eq.(4) denotes inertial term, pressure gradient term and viscosity term, respectively. According to the mass conservation in the process of liquid film drainage, the viscosity term can be converted as follows[34]:

$$\frac{\partial}{\partial r}\left(\frac{1}{r}\frac{\partial}{\partial r}(ru) \right) + \frac{\partial^2 u}{\partial z^2} = 4\left(\frac{\partial^2 u}{\partial r^2} + \frac{1}{r}\frac{\partial u}{\partial r} - \frac{\partial u}{\partial r} - \frac{u}{u^2} \right) + \frac{2}{h}\frac{\partial h}{\partial r}\left(\frac{2\partial u}{\partial r} + \frac{u}{r} \right) \tag{5}$$

In addition, P in Eq.(4) is the average axial pressure in the liquid film, which can

be expressed as follows:

$$P = \frac{2\sigma}{R} - \frac{\sigma}{2}\left(\frac{\partial^2 h}{\partial r^2} + \frac{1}{r}\frac{\partial h}{\partial r}\right) + \Pi \tag{6}$$

Where, σ is the surface tension and R is the equivalent radius, $R=2R_1R_2/(R_1+R_2)$. The use of equivalent radius can extend the model to the collision between fluid particles of non-equal size or between fluid particles and infinite interface. The intermolecular force of Van der Waals $\Pi=A_H/6\pi h^3$ is considered in Eq.(6), where A_H is the Hanmark constant (~10^{-20}J), it can be seen that when the thickness of the liquid film is reduced to ~100nm, the microscopic force cannot be ignored (which will be discussed in Section 4).

2.2 Immobile interface model

Following the work of Klaseboer *et al.*[37], another model of liquid film drainage is given here. On the basis of hypothesis (3), it is considered that the deformation region of liquid film interface has a small slope ($\partial h/\partial r << 1$), so the Reynolds lubrication approximation can be applied to the momentum equation. From the lubrication approximation, the inertia and time derivation terms in the momentum equation (Eq.(2)) can be ignored ($u\frac{\partial u}{\partial r} \approx 0$, $\frac{\partial u}{\partial t} \approx 0$). Combining the assumption (4) mentioned above, Eq.(2) can be simplified to the following form.

$$\frac{\partial P}{\partial r} = \mu_c \frac{\partial^2 u}{\partial z^2} \tag{7}$$

For the immobile interface, u=0 at $z = \pm h/2$. Integrating Eq.(7) twice along the z direction, an expression of the drainage velocity inside the liquid film in the case of immobile interface can be obtained:

$$u = \frac{1}{2\mu_c}\frac{\partial P}{\partial r}\left(z^2 - \left(\frac{h}{2}\right)^2\right) \tag{8}$$

Eq.(8) is generally understood as a parabolic velocity profile driven by a pressure gradient inside the liquid film.

Substituting Eq.(8) into Eq.(1), and then integrating Eq.(1) along the z direction,

the film drainage equation of immobile interface can be obtained:

$$\frac{\partial h}{\partial t}=\frac{1}{12\mu_c r}\frac{\partial}{\partial r}\left(rh^3\frac{\partial P}{\partial r}\right) \tag{9}$$

The pressure P, here, is the same as Eq.(6).

2.3 Initial and boundary conditions

When two spherical fluid particles are just in contact, but no obvious deformation occurs, the corresponding initial film thickness can be defined as:

$$h_0=h_{00}+\frac{r^2}{R} \tag{10}$$

Here h_{00} is the thickness at the center of liquid film at the initial moment.

The drainage velocity of liquid film at the initial time can be calculated as follows:

$$u_0=\frac{rU_{rel,0}}{2h_0} \tag{11}$$

$U_{rel,0}$ is the relative approach velocity between two fluid particles at the initial moment.

At the boundary far away from the liquid film region, there is the following relation (r=r_{bound}):

$$\frac{\partial h}{\partial t}=-U_{constant} \tag{12}$$

$$P=\frac{2\sigma}{R}-\frac{\sigma}{2}\left(\frac{\partial^2 h}{\partial r^2}+\frac{1}{r}\frac{\partial h}{\partial r}\right)=0 \tag{13}$$

If the time-dependent variation of approach velocity at the boundary is considered, Eq.(12) becomes:

$$\frac{\partial h}{\partial t}=-U_{rel}(t) \tag{14}$$

Here $U_{rel}(t)$ is a function of time, it can be obtained from the force balance during the collision of fluid particles. The next section will introduce an approach model of fluid particles to study the effect of variable-velocity boundary conditions on liquid film drainage.

2.4 Approach model

Pressure gradient in the liquid film is the main force driving the liquid film to drain. Under the action of other forces (such as buoyancy and drag force), the pressure distribution in the liquid film will be affected, thus affecting the process of liquid film drainage. However, the approach model proposed by Svendsen and Luo[28] could not reflect the change of pressure in the liquid film. Therefore, it is necessary to consider the influence of pressure gradient on the interface of deformable liquid film in the approach equation.

As shown in Fig.1, the force balance equation based on Newton's second law along the line direction of the fluid particle's center of mass is as follows:

$$\frac{4}{3}\pi R_i^3(\rho_d + C_{VM}\rho_c)\frac{d\boldsymbol{U}_i}{dt} = \boldsymbol{F}_i + \boldsymbol{F}_{C,i} + \boldsymbol{F}_{D,form,i} + \boldsymbol{F}_{Drag,i} \tag{15}$$

Here, $\boldsymbol{U}_i$ is the average flow velocity of the center of mass of bubble i (i=1, 2) relative to the surrounding continuous phase. The term on the left hand side of Eq.(15) is the inertial force containing the contribution of virtual mass force, where ρ_c and ρ_d are the density of continuous phase and the density of fluid particles, respectively. C_{VM} is the virtual mass coefficient, and its value of spherical bubbles of constant size[44] could be taken as 0.5. The physical meaning and expression of the right hand side term of Eq. (15) are as follows:

$$\left|\boldsymbol{F}_i\right| = \frac{4}{3}\pi R_i^3\left(\rho_c - \rho_d\right)g \qquad (Buoyancy\ force) \tag{16}$$

$$\left|\boldsymbol{F}_{Drag,i}\right| = \pi R_i^2 C_{D,i}\frac{\rho_c U_i^2}{2} \qquad (Drag\ force) \tag{17}$$

$$\left|\boldsymbol{F}_C\right| = 2\pi\int_0^{r_f} Prdr \qquad (Capillary\ force) \tag{18}$$

$$\boldsymbol{F}_{D,form} \approx F_C \qquad (Lubrication\ \ force) \tag{19}$$

Here, Eq.(19) arises from extreme cases where lubrication is considered only as a contribution of excess pressure[29]. Regarding the drag coefficient $C_{D,i}$ in Eq.(17), a modified expression proposed by Gong *et al.*[45] is adopted in this paper.

Taking into account the force direction of each fluid particle, Eqs.(16)~(19) are introduced into the force balance equation Eq.(15), and the motion equation of each fluid particle can be obtained:

$$\frac{4\pi}{3}R_1^3\left(\rho_d+C_{VM}\rho_c\right)\frac{dU_1}{dt}=F_1-4\pi\int_0^{r_f}Prdr-\pi R_1^2C_{D,1}\frac{\rho_cU_1^2}{2} \tag{20}$$

$$\frac{4\pi}{3}R_2^3\left(\rho_d+C_{VM}\rho_c\right)\frac{dU_2}{dt}=F_2+4\pi\int_0^{r_f}Prdr-\pi R_2^2C_{D,2}\frac{\rho_cU_2^2}{2} \tag{21}$$

By subtracting Eq.(20) from Eq.(21) and adding Eqs.(20) and (21), respectively, the velocity equation of the two fluid particles approaching each other and the equation of the mass center migration of the two-fluid particle system are finally obtained:

$$\begin{aligned}\frac{\mathrm{d}U_{rel}}{\mathrm{d}t}=&\frac{3}{4}\frac{\left(F_1-\xi^3F_2\right)}{\left(\rho_d+C_{VM}\rho_c\right)\pi R_1^3}-3\left(1+\xi^3\right)\frac{\int_0^{r_f}Prdr}{\left(\rho_d+C_{VM}\rho_c\right)R_1^3}\\&-\frac{3\mu_c}{16\left(\rho_d+C_{VM}\rho_c\right)R_1^2}\left(C_{D,1}U_1Re_1-C_{D,2}U_2\xi^2Re_2\right)\end{aligned} \tag{22}$$

$$\frac{\mathrm{d}U_{mc}}{\mathrm{d}t}=\frac{3}{4}\frac{\xi^3}{\left(1+\xi^3\right)}\frac{\left(F_1+F_2\right)}{\left(\rho_d+C_{VM}\rho_c\right)\pi R_1^3}-\frac{3\mu_c\xi^2\left(\xi C_{D,1}U_1Re_1+C_{D,2}U_2Re_2\right)}{16\left(1+\xi^3\right)\left(\rho_d+C_{VM}\rho_c\right)R_1^2} \tag{23}$$

$$U_1=U_{mc}+\frac{U_{rel}}{\left(1+\xi^3\right)}\qquad U_2=U_{mc}-\frac{\xi^3U_{rel}}{\left(1+\xi^3\right)} \tag{24}$$

Here, U_{rel} (=U_1-U_2) is the relative velocity in the direction of connection line of mass centers of two fluid particles, U_{mc} is the velocity of the mass center of the whole two-fluid particle system, ξ is the ratio of the radius of the two bubbles (=R_1/R_2), and $Re_i=\rho_c d_i U_i/\mu_c$($i$=1,2) is the Reynolds number for the fluid particles, d_i is the diameter of fluid particle i.

The approach model (Eqs.(22)~(24)) can be coupled with the liquid film drainage model (i.e. fully mobile interface model or immobile interface model) through Eq.(14), and the influence of the forces of each component on the liquid film drainage can be analyzed.

3. NUMERICAL PROCEDURE

Different solution strategies are used for the liquid film drainage models of the

two types of mobility interfaces described in Section 2. For the solution of the immobile interface model (Eqs.(7)~(9)), all spatial derivatives use a discrete format of second-order accuracy on a one-dimensional uniform mesh. Starting from Eq.(10), given the initial value h_0 of the film thickness, the pressure P is calculated from Eq.(6). Now that the pressure P is known, the film thickness h at the next moment can be obtained from Eq.(9) in combination with the boundary conditions Eq.(12) (or Eq.(14)) and Eq.(13). When considering the boundary conditions of constant velocity approach, the fixed relative approach velocity $U_{constant}$ between the two fluid particles on the right hand side of Eq.(12) is used. When considering the effect of non-constant velocity approach on liquid film drainage, given an initial relative approach velocity $U_{rel}(t=0)$, Eqs.(22)~(24) can provide a relative approach velocity U_{rel} that changes with time for the drainage model through the boundary condition Eq.(14).

For the fully mobility interface model (Eqs.(3)~(5)), the solution is more complicated, because the model is less simplified. In the drainage velocity equation Eq.(4), inertia term, viscosity term and pressure gradient term in the r direction are retained at the same time. It is foreseeable that this kind of model may obtain more detailed information during the film drainage process. However, as can be seen from Eqs.(4) and (5), the simultaneous existence of inertial and viscous terms makes the drainage velocity equation have more nonlinear terms, which makes the model more difficult to be solved. Unlike the solution of the immobile interface model, an adaptive moving mesh method[46] is applied to the solution of the fully mobile interface model.

During the solution of the adaptive moving mesh method, the total number of mesh nodes is always fixed, and the mesh nodes can migrate to specific areas (such as the area with large curvature of liquid film surface), so as to improve the local mesh resolution. In order to achieve a targeted migration of mesh nodes, it is necessary to couple the mesh density function and the moving mesh partial differential equation (MMPDE) (or moving mesh equation) with the drainage model to be solved. This paper uses an optimal mesh density function (Eq.(25)) and MMPDE4 (Eq.(27)).

$$\hat{\rho}\left(x,t\right)=\left(1+\frac{1}{\alpha_h}\left|\frac{\partial^2 h}{\partial x^2}\right|^2\right)^{\frac{1}{3}} \tag{25}$$

$$\alpha_h=\max\left\{1,\left[\frac{1}{b-a}\int_a^b\left|\frac{\partial^2 h}{\partial x^2}\right|^{\frac{2}{3}}dx\right]^3\right\} \tag{26}$$

$$\frac{\partial}{\partial\zeta}\left(\hat{\rho}\frac{\partial x_t}{\partial\zeta}\right)=-\frac{1}{\tau}\frac{\partial}{\partial\zeta}\left(\hat{\rho}\frac{\partial x_t}{\partial\zeta}\right) \tag{27}$$

In Eqs.(25) and (26), $\hat{\rho}\left(x,t\right)$ is the mesh density function, h is the thickness of the liquid film, [a, b] is the left and right boundary of the physical domain [r_0, r_{bound}], α_h is the adaptive intensity parameter, its value determines the degree of the influence of the derivative of h on the mesh adaptation. In Eq.(27), $\tau(\tau > 0)$ is the mesh response time, the smaller its value is, the more quickly the mesh node can make the corresponding migration. This work chooses τ=10^{-7}. x and ζ are spatial variables, $x_t \equiv \frac{\partial x(\zeta,t)}{\partial t}$. $x(\zeta\ ,t)$ is the mapping of uniform mesh nodes in the computational domain Ω_c on the physical domain Ω, which is obtained through a coordinate transformation:

$$x=x\left(\zeta,t\right):\zeta\in\Omega_c\equiv\left[0,\ell\right]\rightarrow x\in\Omega\equiv\left[a,b\right] \tag{28}$$

The initial and boundary conditions of Eq.(27) are

$$x\left(\zeta,0\right)=\frac{\left(\mathrm{b}-\mathrm{a}\right)\zeta}{\ell}+a \tag{29}$$

$$x\left(0,t\right)=a \qquad x\left(\ell,t\right)=b \tag{30}$$

Eq.(29) indicates that when t=0, uniform mesh is taken as the start of numerical calculation in the physical domain.

Thus, in order to apply the adaptive moving mesh method, the derivatives of Eqs.(3)~(5) in the physical domain can be converted to the computational domain by using the chain rule. In the computational domain, combining the initial conditions (Eqs.(10), (11) and (29)) and boundary conditions (Eq.(12) or Eq.(14), Eqs.(13) and

(30)), the fully mobile interface model and MMPDE4 are solved simultaneously. As with the immobile interface model, the discretization of spatial derivatives uses a central difference scheme with second order accuracy. When the variable-velocity boundary condition Eq.(14) is used, Eqs.(22)~(24) need to be solved simultaneously with Eqs.(3)~(5).

4. RESULTIS AND DISCUSSION

4.1 Constant velocity approach

In the actual process, there are obvious differences in the velocity distribution of flow field in the unit equipment. For example, in a stirred tank, there is a relatively large flow velocity of fluid near the blade, and the collision velocity between fluid particles may also be large, while at the liquid surface or near the wall, the flow velocity of fluid is usually relatively small, and the collision velocity between fluid particles may be relatively low. Due to the different collision velocities, there may be some differences in the process of liquid film drainage and film rupture.

In this work, we focus on the film drainage process of two bubbles. That is, water-air system is considered. Here, ρ_c=998kg/m^3, ρ_d=1.25kg/m^3, μ_c=0.001Pa·s, σ=0.0725N/m. Fig.2 shows time evolution of the liquid film thickness under different constant velocity boundary conditions using the liquid film drainage model with a fully mobile interface (Eqs.(3)~(5)). Fig.3 is the pressure distribution in the liquid film at different moments corresponding to Fig.2. In Fig.2(a), two equal-sized bubbles approach each other at a constant velocity of 0.01m/s. In this case, the inertial term (i.e. the first term on the right hand of Eq.(4)) is relatively weak, and the viscous term dominates the drainage process. As the liquid held between two bubbles is continuously squeezed out, the liquid film is thinning with time and Van der Waals force increases gradually (~1/h^3). The attraction between fluid molecules becomes significant before the capillary pressure plays a major role (The capillary pressure becomes important only when the film radius is enough large). It can be seen from Fig.3(a) that the maximum value of pressure in the liquid film at different times is always maintained at the center of the liquid film. At t=5.17ms, the pressure surges to

about 440Pa, which is because Van der Waals force (Π) is considered in the pressure term in Eq.(6). When the thickness of the liquid film is reduced to the nanometer level, Van der Waals force will play a pivotal role, so that the liquid film rupture at r=0 eventually. Abid and Chesters[42] called this type of liquid film rupture as nose rupture, while rupture occurs at the point deviating from center of the liquid film is called rim rupture. In this work, the occurrence of coalescence (or film rupture) is determined by the relationship between h_{min} and h_{cr}. That is, coalescence (or film rupture) occurs when $h_{min} \leq h_{cr}$ and rebound occurs when $h_{min} > h_{cr}$. Here, h_{min} and h_{cr} denote the minimum thickness of liquid film and the critical thickness for rupture, respectively. An empirical formula of critical thickness proposed by Chesters[47] was used in this work.

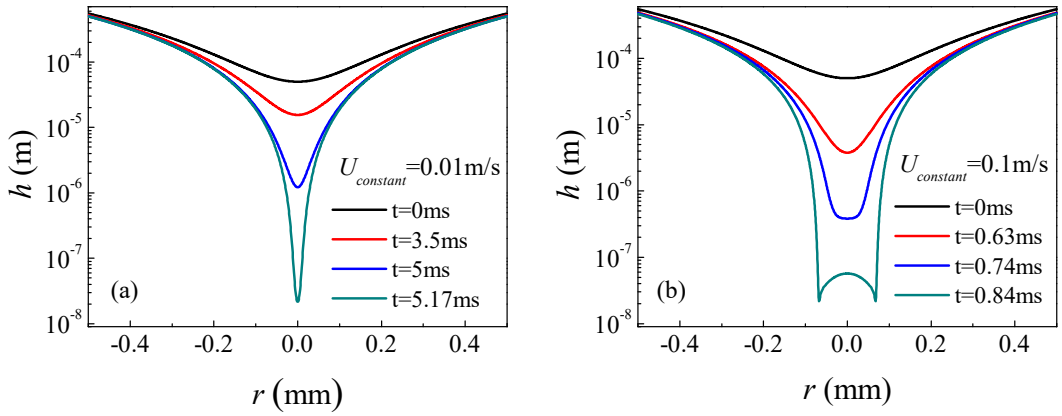

Fig.2 Comparison of time evolution of liquid film thickness at different constant approach velocities (water-air system, ξ=1.0, R_1=0.5mm, h_{00}=0.1R_1, r_{bound} =R_1).

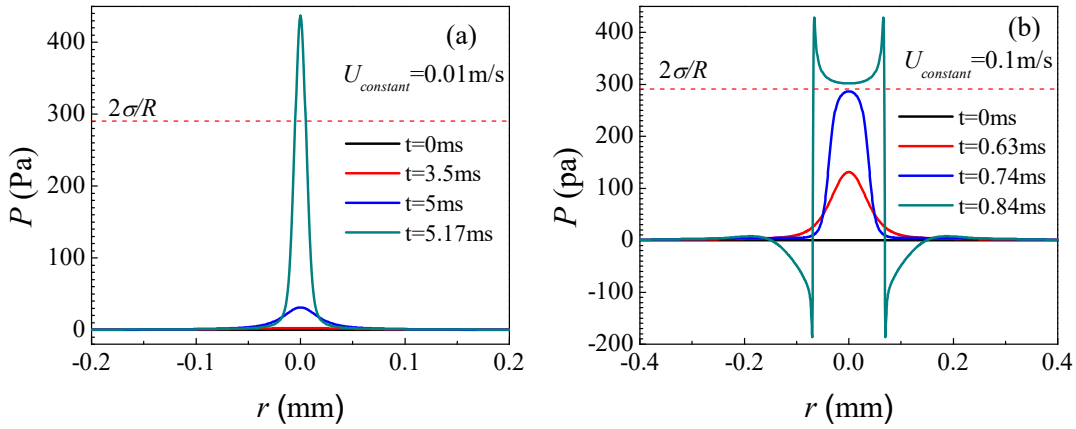

Fig.3 Comparison of pressure distributions in the liquid film at different constant approach velocities (water-air system, ξ=1.0, R_1=0.5mm, h_{00}=0.1R_1, r_{bound} =R_1).

A typical rim rupture is shown in Fig.2(b). Under the constant velocity boundary condition of $U_{constant}$=0.1m/s, the liquid film has undergone a period of flat film drainage (0~0.74ms), and then enters the curved film drainage stage (t>0.74ms). In Fig.3(b), when t>0.74ms, the pressure distribution in the liquid film is greater than the Laplace pressure $2\sigma/R$, and the pressure at edge of the film is greater than the pressure at center of the liquid film, thus forming a curved liquid film. On the outside of the curved liquid film region, there is a negative pressure zone, indicating that a part of the liquid returns to the liquid film to prevent the thinning of the liquid film. On the other hand, a large approach velocity has a strong inertial effect, and the curved liquid film is more likely formed at the liquid film interface. For water-air systems with low viscosity, under the constant velocity boundary condition of $U_{constant}$ =0.1m/s, the inertial term mainly contributes to the liquid film drainage, and the film drainage velocity is faster than that of $U_{constant}$=0.01m/s. Therefore, Fig.2(b) shows a shorter coalescence time (0.84ms).

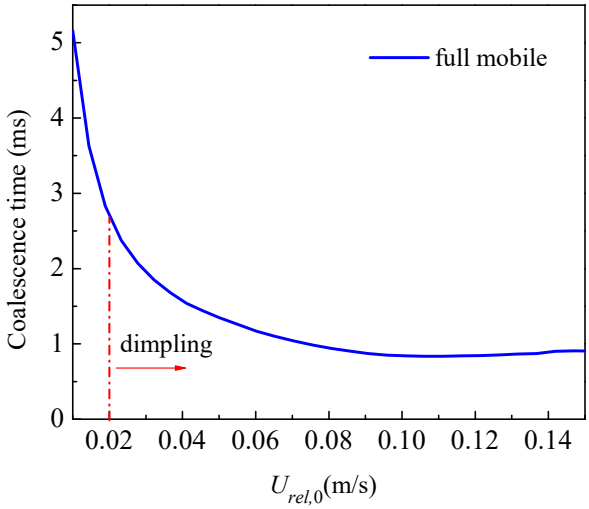

Fig.4 Coalescence time for the fully mobile interface at different constant approach velocities (water-air system, $U_{rel,0}$=$U_{constant}$, ξ=1.0, R_1=0.5mm, h_{00}=0.1R_1, r_{bound} =R_1).

Fig.4 shows the coalescence time of two bubbles with radius of 0.5mm at different constant approach velocities. It can be inferred from Fig.2 that there is a critical velocity U_{dimp} between nose rupture and rim rupture. When it is greater than this value, dimple appears in the liquid film, the type of liquid film rupture is rim

rupture, and otherwise, it is nose rupture. In Fig.4, U_{dimp} is 0.02m/s. When $U_{constant}<U_{dimp}$, the coalescence time decreases almost linearly with the increase of approach velocity. When $U_{constant}>U_{dimp}$, the dimple becomes significant, and the tendency of coalescence time to decreasing with the increasing velocity decreases. It should be emphasized that not colliding bubbles at all velocities will coalesce, in contrary, rebound may occur. It is difficult to predict this phenomenon by using a constant boundary condition for the drainage model, which will be discussed in detail in the next section.

In order to compare the differences between the different drainage models, we investigate the characteristics of the immobile interface model with constant velocity approach under the same condition. Fig.5(a) shows the time evolution of the liquid film thickness. Compared with the fully mobile interface model, no nose rupture is observed in the immobile interface model at the approach velocity of 0.01m/s. Because the model only considers that contribution of parabolic drainage driven by pressure difference to the film thickness thinning, there is a difference of magnitude between this model and the fully mobile interface model. It can be seen from Fig.5(b) that after the formation of a dimple film (t > 9ms), the pressure distribution in the liquid film is basically maintained nearby $2\sigma/R$, and the pressure gradient in the film is quite small, which reveals the reason why the curved liquid film is relatively flat in Fig.5(a). In Fig.5(c), the minimum and central film thicknesses decreases with the increase of time, and remains at 1.38μm after t=35ms. At the same time, the radius of the liquid film gradually increases to 0.19mm with time, which is basically constant, as shown in Fig. 5(d). In our simulation, we cannot predict the evolution information of the liquid film after 10^{-6}m by the immobile interface model with constant velocity boundary condition, so we cannot get the coalescence time of bubbles from this model. For the collision of bubbles in pure water, the film is thinned to nanometer scale, and the time required for bubble coalescence is less than 10ms. Therefore, we consider that this model may not be suitable for physical systems with low viscosity and high Reynolds number. Nevertheless, we can still study the performance of the immobile interface model under different boundary conditions.

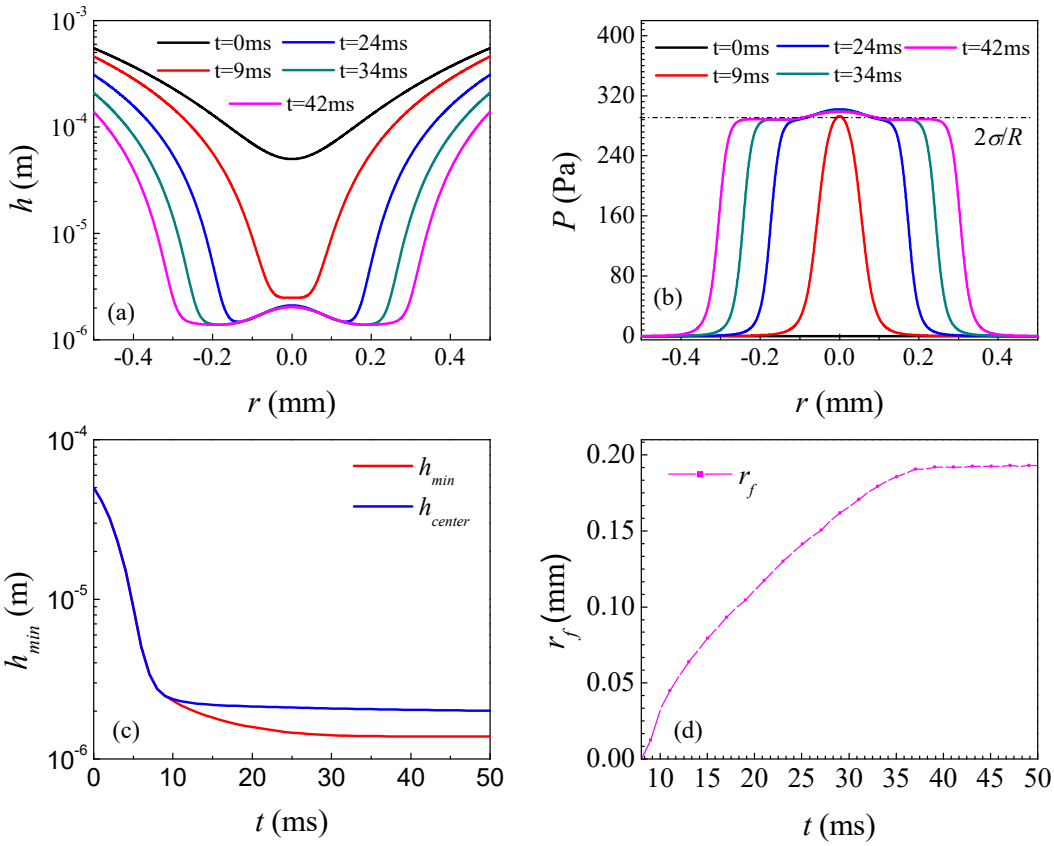

Fig.5 The evolution predicted by immobile interface model at constant approach velocity((a) liquid film thickness, (b) pressure distribution, (c) minimum film thickness and central film thickness, (d) curved liquid film radius)(water-air system, ξ=1.0, R_1=0.5mm, h_{00}=0.1R_1, r_{bound} =R_1).

4.2 Non-constant velocity approach

As mentioned earlier, when two bubbles collide at a certain velocity, they may rebound in addition to coalescence. However, it is difficult to predict the rebound phenomenon through the drainage model with constant velocity boundary conditions, because two fluid particles always approach each other at a constant velocity until they coalesce. In this section, we will consider the variety of bubble relative motion and explore the characteristics of liquid film drainage model under non-constant velocity boundary conditions.

Fig.6 compares the difference of liquid film drainage process predicted by the fully mobile interface model under the constant-velocity and variable-velocity boundary conditions. The results indicate that the drainage velocity of the former is

faster than that of the latter. At the same time, the model with constant approach velocity boundary condition predicts a smaller film thickness. Meanwhile, there is a greater liquid film radius in the dimpled drainage region.

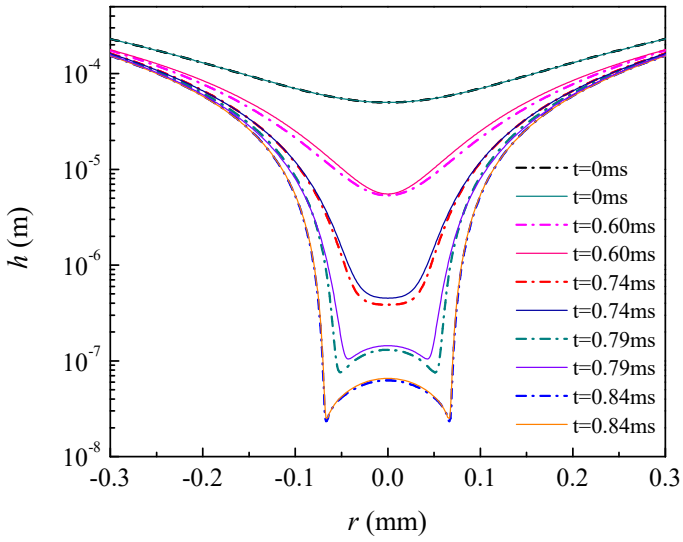

Fig.6 Comparison of liquid film evolution under constant-velocity (dotted line) and variable-velocity (solid line) boundary conditions (water-air system, ξ=1.0, R_1=0.5mm, h_{00}=0.1R_1, r_{bound} =R_1).

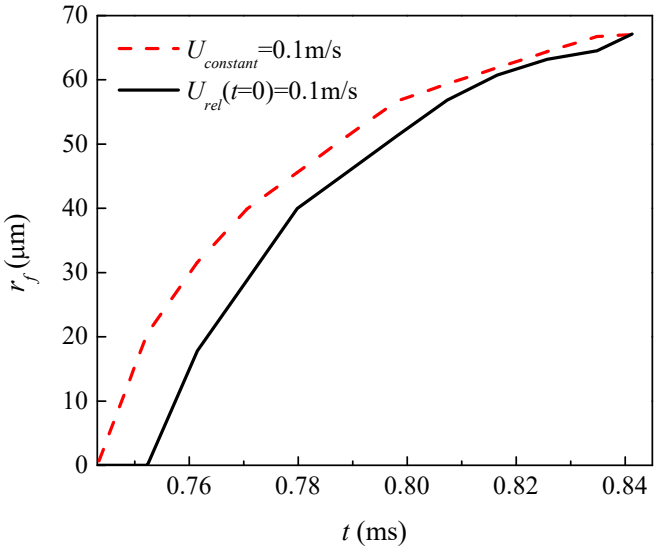

Fig.7 Comparison of evolution of dimple film radius under constant-velocity (dotted line) and variable-velocity (solid line) boundary conditions (water-air system, $U_{constant}$=0.1m/s, ξ=1.0, R_1=0.5mm, h_{00}=0.1R_1, r_{bound} =R_1).

The evolution of dimple film radius under two kinds of boundary conditions is given in Fig.7. It can be clearly seen that in both cases, the dimple film radius r_f gradually increases with time. For the liquid film with constant approach velocity, the curved liquid film appears earlier, so the radius of liquid film is kept larger in the whole process of liquid drainage. Although the coalescence time difference is only 0.01ms, it will become significant with the increase of initial relative approach velocity and bubble size.

The fully mobile interface model with variable-velocity boundary condition predicts a slower drainage velocity, which can be explained by analyzing the force components of the model at different times. Fig.8 shows the evolution of different forms of forces on the liquid film and the evolution of the relative approach velocity U_{rel} at different times. The blue solid line in Fig.8(a) represents the inertial force or the resultant force including the virtual mass force. The black solid line represents the "film force" which denotes a combined action of capillary force, lubrication form drag force and Van der Waals force during the drainage process. When the two bubbles just contact, the distance between the liquid film interfaces is large, the "film force" at the initial stage (0~0.25ms) can almost be ignored, buoyancy can be viewed as a dominant force. Therefore, in Fig.8(b) for 0~0.25ms, the relative approach velocity between bubbles has a slight acceleration. With the thinning of liquid film, the lubrication form drag force increases gradually, the acceleration of U_{rel} slows down correspondingly. After 0.35ms, the lubrication force gradually becomes dominant on the liquid film. Therefore, the inertial force containing a virtual mass gradually increases in the opposite direction of buoyancy, and the relative approach velocity gradually decreases. After 0.75ms, the liquid film force increased sharply because the liquid film drainage entered the dimpled drainage region. At this time, due to the increase of the curvature of the liquid film, the capillary pressure increased rapidly and became a main force to prevent the bubble from approaching further. When the film thickness is less than 100 nm, the attraction between the dense water molecules in the center of film and the thin water molecules in the gas-liquid interface increases gradually, and becomes a key factor for the final film rupture. The

comprehensive effects of buoyancy, lubrication force, capillary force and Van der Waals intermolecular force in the process of liquid film drainage can be reflected in the evolution of relatively approach velocity in Fig.8(b). Therefore, the decrease of approach velocity under the condition of non-constant velocity boundary explains the difference of film thickness evolution in Fig.6.

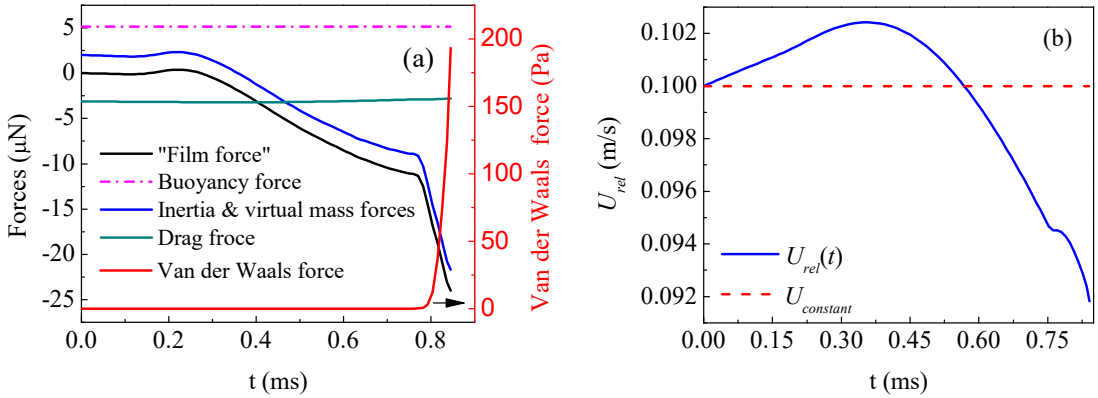

Fig.8 Evolution of the different forces on liquid film (a) and the relative approach velocity under variable-velocity boundary condition (b) (water-air system, $U_{constant}$=0.1m/s, ξ=1.0, R_1=0.5mm, h_{00}=0.1R_1, r_{bound} =R_1).

In order to study the discrepancy of different boundary conditions on the immobile interface model, the same case as Fig.5 in the previous section is investigated by using the non-constant velocity boundary condition. Fig.9 shows the time evolution of liquid film thickness and pressure distribution in the film. Compared with Fig.5(a), the time evolution of liquid film thickness in Fig.9(a) shows not only dimple (t=14.7ms) but also wimple (t=13.7ms) and pimple (t=12.9ms). A detailed definition of the different shapes of the liquid film interface can be found in section 3.1.2 of Chan *et al*.[24] In fact, the change of interface shape of the liquid film is related to the surface restoring force of the fluid particles and the distribution of the pressure in the liquid film along the radial positions. The fluid flow in a liquid film is driven by the pressure gradient, whereas the overall variation of buoyancy, drag force and "film force" will affect the pressure distribution in the liquid film. It can be seen that, compared with Fig.4(b), the time evolution of pressure distribution in the liquid film

changes dramatically under the condition of variable velocity boundary, in Fig.9(b). When t=12.9ms, the pressure outside the edge of the liquid film is negative, forming a pimple interface, which is consistent with the theoretical derivation of Chan *et al.*[27] Similar to Fig.3(b), the existence of negative pressure zone near rim liquid film leads to an attractive hydrodynamic inside the liquid film, which resists the liquid inside the film from being extruded out. Different from the fully mobile interface, as the negative pressure zone increases, wimple and dimple are formed in the immobile interface in Fig.9(b), which may be related to the slow drainage velocity and bounce at the boundary far away from the liquid film area. Meanwhile, it is noted that because the thickness of the liquid film is difficult to reach the critical film thickness of nanometer scale, the rebound phenomenon has begun to appear outside the liquid film areas at t=12.9~14.7ms. In Fig.10, the minimum film thickness h_{min}, predicted by the immobile interface model, is plotted as a function of time. It can be seen that the minimum film thickness reached in the drainage process increases significantly after t=14.7ms, which reveals that the drainage model can better predict rebound phenomenon by considering the variable-velocity approach boundary condition.

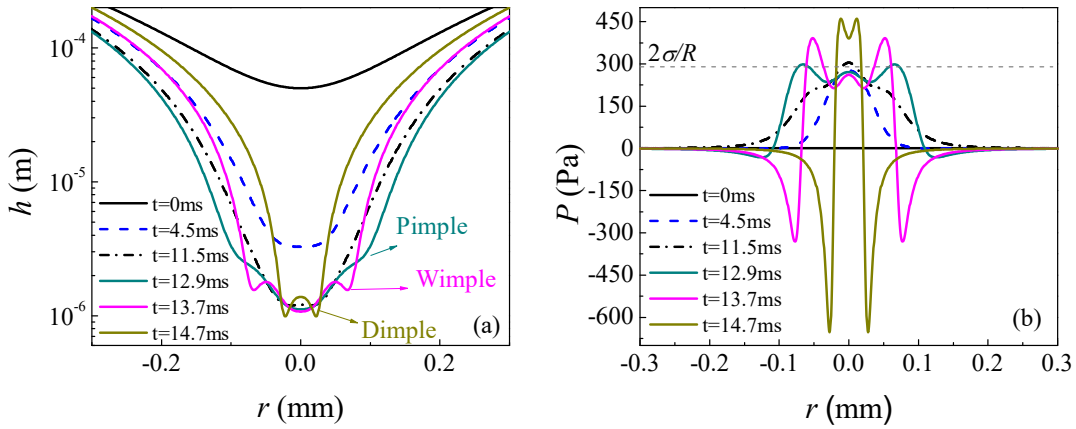

Fig.9 The evolution of liquid film thickness (a) and pressure distribution in the liquid film(b) predicted by the immobile interface model with the boundary condition of non-constant approach velocity (water-air system, U_{rel} (t=0)=0.01m/s, ξ=1.0, R_1=0.5mm, h_{00}=0.1R_1, r_{bound} =R_1).

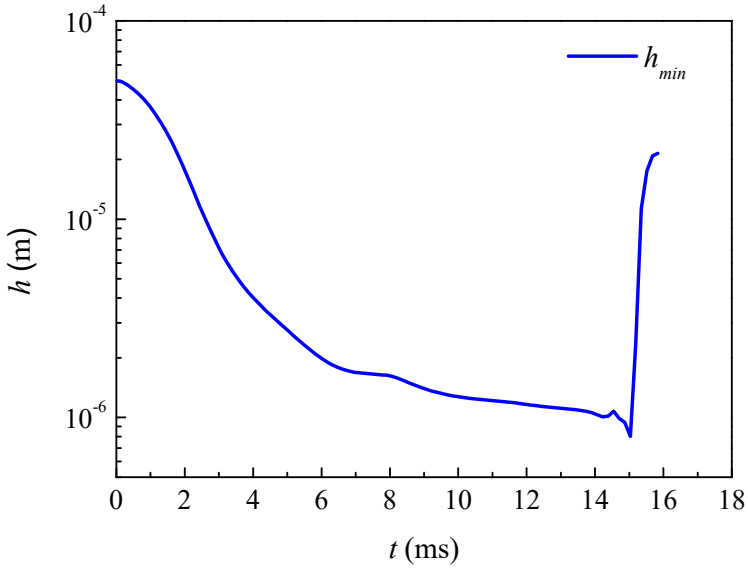

Fig.10 Evolution of the minimum film thickness predicted by the immobile interface model with a non-constant approach velocity (water-air system, $U_{rel}(t=0)$=0.01m/s, ζ=1.0, R_1=0.5mm, h_{00}=0.1R_1, r_{bound} =R_1).

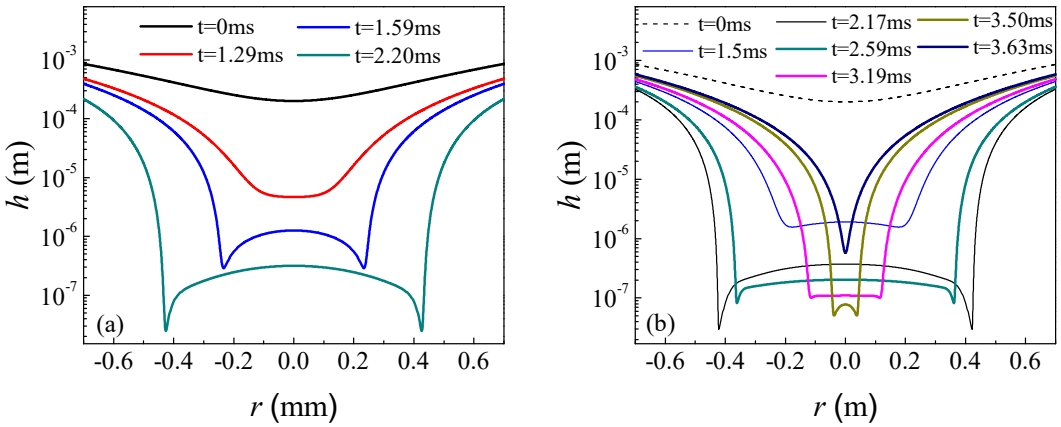

Fig.11 Evolution of the film thickness under different boundary conditions: (a) coalescence occurs under constant-velocity approach, and (b) rebound occurs under non-constant-velocity approach (water-air system, $U_{rel}(t=0)$ or $U_{constant}$= 0.3m/s, ζ=1.0, R_1=0.75mm, h_{00}=0.2mm, r_{bound} =R_1).

Experiments show that when the collision velocity between two bubbles is greater than a critical value, the phenomenon of rebound appears. We use the fully mobile interface model with constant and non-constant velocity boundary conditions,

respectively, to study the collision of two equal-sized bubbles with radius of 0.75mm at a relative velocity of 0.3m/s. Fig.11 shows the time evolution of the film thickness under two boundary conditions. In Fig.11(a), when the boundary condition of constant velocity approach is considered, the film thickness gradually decreases and the radius of dimple increases. Eventually, the film thickness reaches the critical rupture thickness (~25nm) at t=2.20ms, the two bubbles coalesce. Fig.12(a) and Fig.13(a) respectively indicate the evolution of the radius of the dimple and the film thickness at the center h_{center} and the minimum film thickness h_{min} under the boundary condition of constant approach velocity. However, the fully mobile interface model which takes into account the boundary condition of non-constant approach velocity predicts quite different results. In Fig.11(b), from t=0 to t=2.17ms, the decrease of the film thickness and the expansion of the dimple radius show a similar trend as shown in Fig.11(a). After t>2.17ms, the liquid film thickness does not continue to decrease to the critical film thickness, but appears, the liquid film radius begins to gradually shrink (Fig.12(b)), and the minimum film thickness retreated (Fig.13(b)). It is noted that during the initial stage of bubble rebound (t=2.17~3.5ms), the liquid film center is still thinning (Fig.13(b)), because the rebound starts at the boundary far away from the curved liquid film area, and gradually drives the inside area from the outside area.

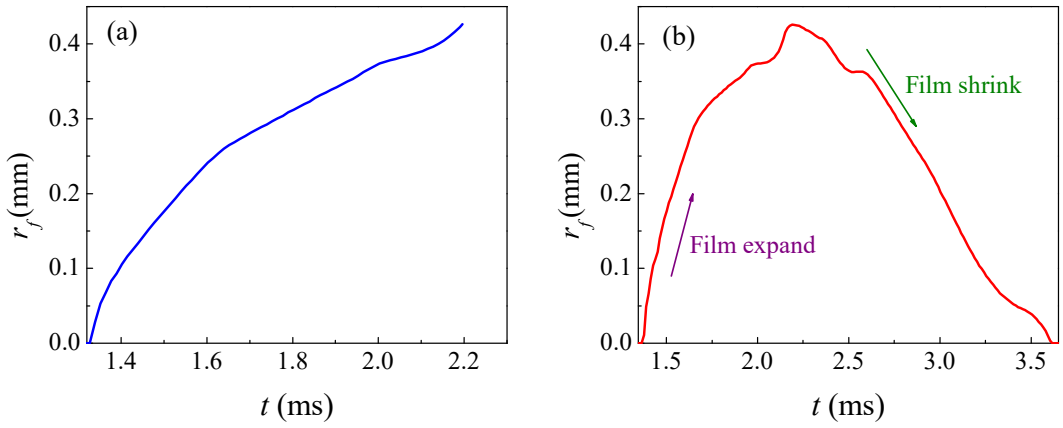

Fig.12 Comparison of evolution of the film radius under constant velocity boundary condition(a) and non-constant velocity boundary condition(b) (water-air system, U_{rel} (t=0) or $U_{constant}$= 0.3m/s, ξ=1.0, R_1=1.0mm, h_{00}=0.2mm, r_{bound} =R_1).

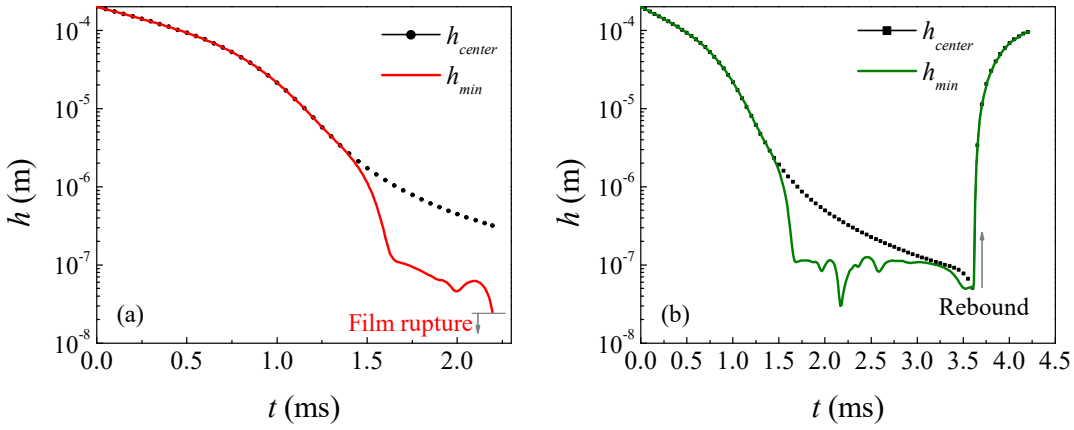

Fig.13 Comparison of the central film thickness and the minimum film thickness under constant velocity boundary condition (a) and non-constant velocity boundary condition(b) (water-air system, U_{rel}(t=0) or $U_{constant}$= 0.3m/s, ξ=1.0, R_1=1.0mm, h_{00}=0.2mm, r_{bound} =R_1).

Fig.12(b) shows in detail the process of the dimple radius extending from 0 to the maximum value of 0.43mm, and then shrinking from the maximum value to 0. The disappearance of the curved liquid film means that the minimum film thickness returns to the center of the liquid film. In Fig.13(b), after t=3.5ms, the center of the liquid film and the minimum liquid film thickness basically coincide, and the liquid film rebounds rapidly to an order equivalent to the initial film thickness, indicating that the two bubbles have basically completed rebound. Fig.14 is the time evolution of the relative approach velocity U_{rel} of two bubbles. In the collision process of two bubbles, U_{rel} gradually decreases to 0 with time, and starts to accelerate in the reverse direction of approach after t=2.24ms. The reverse movement of the bubbles is fed back to the liquid film area through the boundary condition, and eventually the liquid film will gradually become thicker and the two bubbles will separate from each other.

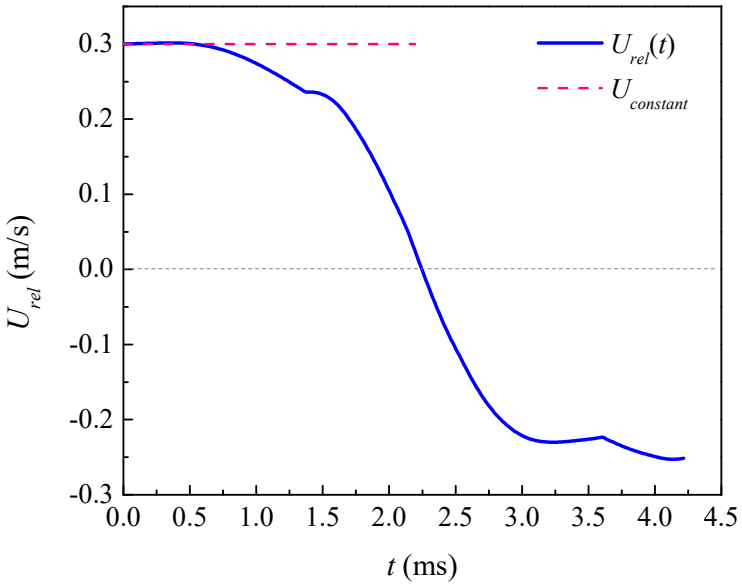

Fig.14 The time evolution of relative approach velocity (water-air system, $U_{rel}(t=0)$ or $U_{constant}$= 0.3m/s, ξ=1.0, R_1=1.0mm, h_{00}=0.2mm, r_{bound} =R_1).

4.3 Comparison of the model results and the experiments

In order to verify the prediction ability of the drainage model under different boundary conditions, we conducted an experimental comparison. The coalescence and rebound of two equal-sized bubbles in head-on collision were recorded by a high-speed camera, with frame rate of 5000 fps. In static ultra-pure water, a bubble is first released through a micro-syringe. After traveling a distance, the bubble is trapped by a capillary. Through the appropriate operation, the trapped bubble can be finally still (please see Fig.15(a)) due to that the buoyancy of bubble (i.e. F_2 in Eqs.(23) and (24)) balances the supporting force of the capillary tube ($F_{\text{supporting}}$) to the bubble. And then, a second bubble of the same size is then released and the two bubbles collide head-on, driven by buoyancy (i.e. F_1 in Eqs.(23) and (24)). In the case of head-on collision, the effect of $F_{\text{supporting}}$ and F_2 on the collision process could be ignored because $F_{\text{supporting}}$ is approximately balanced by F_2. Correspondingly, $F_{\text{supporting}}$ does not appear in Eqs.(23) and (24), and F_2 is taken as zero. However, for the offer-center collision of two bubbles, this effect should be considered in the approach model. This work only focuses on the case of head-on collision of bubbles.

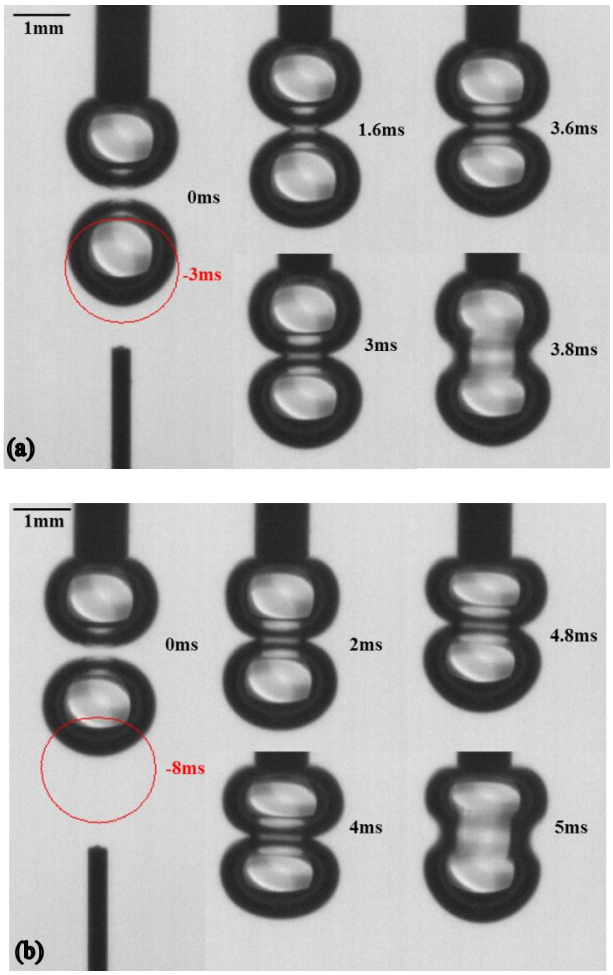

Fig.15 Image sequence of collision of two bubbles (ξ=1, R_1=1.0mm) in water recorded by high-speed camera. Case (a): the initial collision velocity $U_{collision}$ (i.e. U_{rel} (t=0)) is 0.15m/s, and coalescence occurs at t~3.6ms; Case(b): $U_{collision}$= 0.20m/s, and coalescence occurs at t~4.8ms.

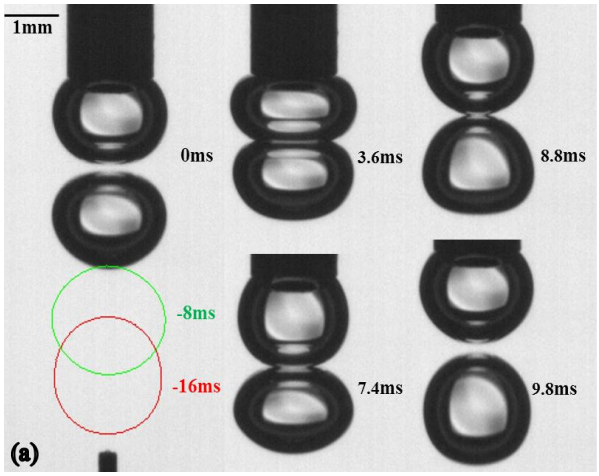

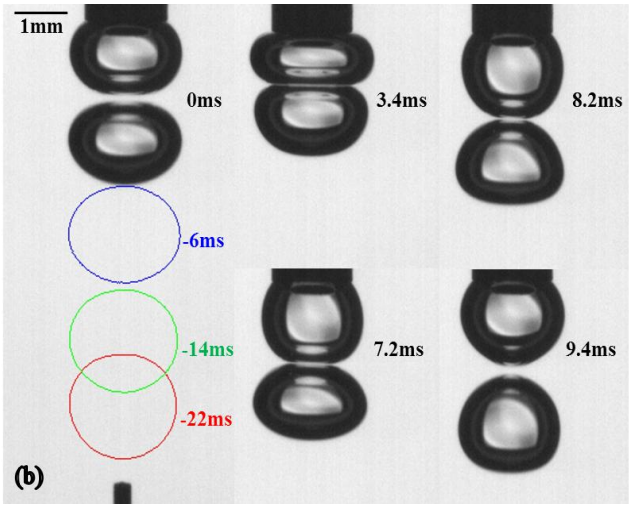

Fig.16 Image sequence of collision of two bubbles with radius of 1.0mm in water recorded by high-speed camera. Case(a): $U_{collision}$ =0.278m/s , and bounce occurs after t~8.8ms; Case(b): $U_{collision}$= 0.304m/s, and bounce occurs after t~8.2ms.

Fig.15 and Fig.16 show the image sequences of coalescence and rebound of two equal-sized bubbles with radius of 1.0 mm. In order to obtain the coalescence time of the bubbles, the time when two bubbles are in initial contact is defined as 0ms, and the corresponding rising time before the bubbles are contacted is defined as a negative value. Fig.15(a) and Fig.15(b) respectively represent the cases in which the bubbles collide at the initial time with the relatively approach velocity U_{rel} at 0.15m/s and 0.20m/s, and eventually coalesce at about 3.6ms and 4.8ms. Cases of bubbles of the same size as those in Fig.15, but collide at a higher relative approach velocity (0.278m/s or 0.304m/s) and eventually rebound, can be observed in Fig.16. Combining the cases of bubble coalescence and rebound in Fig.15 and Fig.16, we compare the model prediction results with the experiments. For convenience, the constant velocity boundary condition is denoted as C, the variable velocity boundary condition as V, the fully mobile interface model as M, and the immobile interface model as I. Now, the two models can be combined with different boundary conditions. For example, the M & C represents the fully mobile interface model with constant velocity boundary condition. The comparison between the simulation results of different combinations of the models and the experiments is summarized in Table 1. The thickness of the liquid film center (h_{00}) at the initial moment in each case is also

Table 1. Comparison of the prediction results and the experiments (ρ_c=998kg/m^3 ρ_d=1.25kg/m^3, μ_c=0.001Pa·s, σ=0.0725N/m, A_H=3.719×10^{-20}J, ξ=1, r_{bound} =R_1)

R_1 (mm)	h_{00} (mm)	U_{rel}(t=0) (m/s)	Coalescence | Coalescence time (ms)				
			Exp.	M & C	I & C	M & V	I & V
1.0	0.13	0.15	Yes | 3.6	Yes | 3.19	No	Yes | 3.01	No
	0.10	0.20	Yes | 4.8	Yes | 4.43	No	Yes | 4.42	No
	0.13	0.278	No	Yes | 4.10	No	No	No
	0.15	0.304	No	Yes | 3.78	No	No	No

listed in Table 1. It is worth noting that h_{00} is a key parameter, and its value will affect the coalescence time and even the result of collision. Unfortunately, there is no general way to determine this value. In order to get a good prediction results, some researchers choose to use 0.1 ~ 0.2R. Different from this rough method, we measured the distance between the bubble interfaces when two bubbles just contacted as the initial film thickness. Although this method is cumbersome, it can provide a more realistic physical value.

In the Table 1, it can be found that I & C and I & V are less capable of predicting coalescence events in water-air system because this model has a slower film drainage velocity, which has been discussed in the previous section. Instead, both M & V and M & C can successfully predict the coalescence of two bubbles when the initial approach velocity is low. Furthermore, we benchmark the moment when two bubbles appear apparent coalescence (e.g. Fig.15(a), 3.8ms), one frame forward is taken as the coalescence time. Although the liquid film may have ruptured earlier, the liquid film rupture is instantaneous, so this treatment is feasible. In the two cases of bubble coalescence with initial approaching velocity of 0.15m/s and 0.20m/s, M & V and M & C can reasonably predict the coalescence time of bubbles. The reason why the coalescence time predicted by the M model is slightly less than that observed by experiment may be due to the fact that the fully mobile interface model has a faster liquid drainage rate and the bubbles have a certain degree of deformation. On the other hand, it may be due to the limitation of experimental observation accuracy,

which results in a higher coalescence time recorded.

When the bubbles collide at a higher velocity, they are more likely to bounce back than coalescence. For the two cases of bubble collision at higher velocities shown in Fig.16, M & V well predicts the occurrence of bubble bounces, whereas M & C seems to be more likely to overestimate the coalescence ability of bubbles in high velocity collisions. It is indicated that the non-constant velocity boundary condition should be considered in the film drainage model. As seen from Table 1, the combination of M & V has a better ability to predict rebound events, which means that the critical coalescence velocity of bubbles can be predicted more reasonably in theory. Critical coalescence velocity is a key parameter for coalescence rate model required in the population balance modeling (PBM), however, is very cumbersome to obtain it by experimental means.

5. CONCLUSIONS

In this work, a coupling framework for modeling the non-constant-velocity approach of two fluid particles and the curved film drainage is developed. Both approach and liquid film drainage processes are considered simultaneously, which provides a more physically meaningful variable velocity boundary condition for the film drainage model. In the improved approach model, besides considering the buoyancy and drag forces of the bubbles, the capillary pressure, lubrication form drag force, and the intermolecular attraction of Van der Waals are also considered. By analyzing the evolution of each component force in the process of bubble collision, the change of the relative approach velocity is quantitatively explained, and then the liquid film drainage process is better understood. The characteristics of two models with different interface mobility under constant velocity boundary and non-constant velocity boundary conditions are studied.

Concretely, under the constant velocity boundary conditions, the simulation results of the fully mobile model show that when Re is less than 20 ($Re = \rho_c dU/\mu_c$), the liquid film drainage is dominated by the viscous term, the liquid film thinning rate is

slower, the coalescence time is longer, and the position of the liquid film rupture appears at the center of the liquid film. As the approach velocity increases, the inertial term begins to work, the liquid film drainage rate is accelerated, the corresponding coalescence time decreases, and the type of drainage is mainly in the dimpled drainage regimes. When *Re* is greater than 100, the coalescence time increases slightly, because the inertia force increases, the curvature of the liquid film increases, and the separation pressure inside the liquid film prevents the thinning of the liquid film. In the gas-liquid system with *Re*>1, which is the focus of this work, it is found that the immobile interface model, whether under constant velocity boundary condition or variable velocity boundary condition, fails to predict the information after the liquid film thickness is reduced to the micron level. Because the liquid in the immobile film is squeezed out, only the parabolic velocity profile driven by pressure contributes, so the film thinning rate is quite slow. Even if a constant velocity boundary condition of 0.01 m/s is set for the immobile interface model, the approaching velocity at the boundary is much greater than the thinning rate of the liquid film area. This may be the reason why the model can't be adapted to the relatively high velocity boundary conditions. On the other hand, the immobile interface model with variable velocity boundary condition starts to rebound when the thickness of liquid film reaches ~10^{-6}m, and in the process of rebound, three types of liquid film mentioned in Chan *et al*.[27] and Ozan and Jakobsen[43], pimple, wimple and dimple, appear.

The simulation results of the fully mobile interface model under the non-constant boundary condition indicate that the film has a slower thinning rate due to the gradual slowing down of the approach velocity. By analyzing the evolution of each component force in the process of bubble collision, the reason of the change of approach velocity is revealed. At the initial stage of bubble collision, the liquid film is thick and the lubrication force and capillary pressure can be ignored. With the thinning of liquid film thickness, the lubrication form drag force gradually increases, and then the formation of curved film will make the capillary pressure become the dominant force to prevent the bubbles from further approaching. Then, when the film thickness is reduced to ~100nm, the Van der Waals attraction will not be ignored. At

higher initial approaching velocity, the models with constant velocity boundary condition and variable velocity boundary condition may predict significantly different results. The latter can better predict the phenomenon of bubble rebound under high-velocity collision, while the former may overestimate the coalescence ability of bubbles, and more predict the occurrence of coalescence. Finally, compared with the experimental results, it is verified that the full mobile interface model with non-constant velocity approach can better predict the coalescence and rebound of bubbles.

Due to the limited experimental data available, there is no more verification on the coalescence time. For further work, the effect of the approach velocity on the liquid film drainage model of partially mobile interface will be considered. In order to obtain the coalescence time required for the verification of the model, more head-on collisions will be carried out.

ACKNOWLEDGMENT

The authors acknowledge the financial support from the National Natural Science Foundation of China (21676224), and the project supported by Scientific Research Found of Hunan Provincial Education Department (18A076).

SUPPLEMENTARY MATERIALS

The videos of Fig.15 and Fig.16 can be found in the supplementary materials.

REFERENCES

1 Lu J, Corvalan CM, Chew YMJ, Huang JY. Coalescence of small bubbles with surfactants. Chem. Eng. Sci. 2019:196:493-500.

2 Merrouche D, Mohammedi K, Belaidi I, Mabrouki B. Simulation of the coalescence of two bubbles rising in a vertical pipe with VOF Interface tracking method. AIP Conference Proceedings. 2007;907:1348.

3 Gross M, Steinbach I, Raabe D, Varnik F. Viscous coalescence of droplets: A

lattice Boltzmann study. Physics of Fluids. 2013;25:052101.

4 Komrakova AE, Eskin D, Derksen JJ. Numerical study of turbulent liquid−liquid dispersions. AlChE J. 2015;61:2618-2633.

5 Lim SJ, Choi MC, Weon BM, Gim B. Lattice Boltzmann simulations for water coalescence. Appl. Phys. Lett. 2017;111:101602.

6 Elghobashi S. Direct numerical simulation of turbulent flows laden with droplets or bubbles. Annual Review of Fluid Mechanics. 2019;51:217-244.

7 Janssen PJA, Anderson PD. Modeling film drainage and coalescence of drops in a viscous fluid. Macromolecular Materials and Engineering. 2011;296:238-248.

8 Howarth WJ. Coalescence of drops in a turbulent flow field. Chem. Eng. Sci. 1964;19:33-38.

9 Coulaloglou CA, Tavlarides LL. Description of interaction processes in agitated liquid-liquid dispersions. Chem. Eng. Sci. 1977;32:1289-1297.

10 Sovová H. Breakage and coalescence of drops in a batch stirred vessel-II comparison of model and experiments. Chem. Eng. Sci. 1981;36:1567-1573.

11 Prince MJ, Blanch HW. Bubble coalescence and break-up in air-sparged bubble columns. AlChE J. 1990;36:1485-1499.

12 Luo HA. Coalescence, break-up and liquid circulation in bubble column reactors. Thesis, 1993.

13 Tsouris C, Tavlarides LL. Breakage and coalescence models for drops in turbulent dispersions. AlChE J. 1994;**40**:395-406.

14 Kamp AM, Chesters AK, Colin C, Fabre J. Bubble coalescence in turbulent flows: A mechanistic model for turbulence-induced coalescence applied to microgravity bubbly pipe flow. Int. J. Multiphase Flow. 2001;27:1363-1396.

15 Lehr F, Millies M, Mewes D. Bubble-size distribution and flow fields in bubble columns. AlChE J. 2002;48:2426-2433.

16 Wang TF, Wang JF, Jin Y. Population balance model for gas-liquid Flows: influence of bubble coalescence and breakup models. Ind. Eng. Chem. Res. 2005; 44:7540-7549.

17 Wang TF, Wang JF, Jin Y. A CFD–PBM coupled model for gas–liquid flows.

AIChE J. 2006;52:125-140.

18 Das SK. Development of a coalescence model due to turbulence for the population balance equation. Chem. Eng. Sci. 2015;137:22-30.

19 Solsvik J, Jakobsen HA. Development of fluid particle breakup and coalescence closure models for the complete energy spectrum of isotropic turbulence. Ind. Eng. Chem. Res. 2016;55:1449-1460.

20 Gong SG, Han LC, Luo HA. A novel multiscale theoretical model for droplet coalescence induced by turbulence in the framework of entire energy spectrum. Chem. Eng. Sci. 2018;176:377-399.

21 Liao Y, Lucas D. A literature review on mechanisms and models for the coalescence process of fluid particles. Chem. Eng. Sci. 2010;65:2851-2864.

22 Venneker BCH, Derksen JJ, Van den Akker HEA. Population balance modeling of aerated stirred vessels based on CFD. AIChE J. 2002;48:673-685.

23 Chen P, Duduković MP, Sanyal J. Three-dimensional simulation of bubble column flows with bubble coalescence and breakup. AIChE J. 2005; 51: 696-712.

24 Li DY, Gao ZM, Buffo A, Podgorska W, Marchisio DL. Droplet breakage and coalescence in liquid-liquid dispersions: Comparison of different kernels with EQMOM and QMOM. AIChE J. 2017;63:2293-2311.

25 Hecht KJ, Krause U, Hofinger J, Bey O, Nilles M, Renze P. Prediction of gas density effects on bubbly flow hydrodynamics: New insights through an approach combining population balance models and computational fluid dynamics. AIChE J. 2018;64: 3764-3774.

26 Zhang XB, Luo ZH. Effects of bubble coalescence and breakup models on the simulation of bubble columns. Chem. Eng. Sci. 2020;226:115850.

27 Chan DYC, Klaseboer E, Manica R. Film drainage and coalescence between deformable drops and bubbles. Soft Matter. 2011;7:2235-2264.

28 Svendsen HF, Luo HA. Modeling of approach processes for equal or unequal sized fluid particles. Can. J. Chem. Eng. 1996;74:321-330.

29 Hagesaether L, Jakobsen HA, Svendsen HF. Theoretical analysis of fluid particle collisions in turbulent flow. Chem. Eng. Sci. 1999;54:4749-4755.

30 Klaseboer E, Manica R, Hendrix MHW, Ohl CD, Chan DYC. A force balance model for the motion, impact, and bounce of bubbles. Physics of Fluids. 2014;26: 092101.

31 Mackay GDM, Mason SG. The gravity approach and coalescence of fluid drops at liquid interfaces. Can. J. Chem. Eng. 1963;41:203-212.

32 Chesters AK. The applicability of dynamic-similarity criteria to isothermal, liquid-gas, two-phase flows without mass transfer. Int. J. Multiphase Flow. 1975;2: 191-212.

33 Oolman TO, Blanch HW. Bubble coalescence in stagnant liquids. Chem. Eng. Commun. 1986;43:237-261.

34 Chesters AK, Hofman G. Bubble coalescence in pure liquids. Appl. Sci. Res. 1982;38:353-361.

35 Saboni A, Gourdon C, Chesters AK. Drainage and rupture of partially mobile films during coalescence in liquid-liquid systems under a constant interaction force. J. Colloid Interface Sci. 1995;175:27-35.

36 Bazhlekov IB, Chesters AK, van de Vosse FN. The effect of the dispersed to continuous-phase viscosity ratio on film drainage between interacting drops. Int. J. Multiphase Flow. 2000;26:445-466.

37 Klaseboer E, Chevaillier JP, Gourdon C, Masbernat O. Film drainage between colliding drops at constant approach velocity: experiments and modeling. J. Colloid Interface Sci. 2000;229:274-285.

38 Yaminsky VV, Ohnishi S, Vogler EA, Horn RG. Stability of aqueous films between bubbles. Part 1. The effect of speed on bubble coalescence in purified water and simple electrolyte solutions. Langmuir. 2010;26:8061-8074.

39 Hendrix MHW, Manica R, Klaseboer E, Chan DYC, Ohl CD. Spatiotemporal evolution of thin liquid films during impact of water bubbles on glass on a micrometer to nanometer scale. Phys. Rev. Lett. 2012;108:247803.

40 Liu B, Manica R, Liu Q, Klaseboer E, Xu Z, Xie G. Coalescence of bubbles with mobile interfaces in water. Phys. Rev. Lett. 2019;122:194501.

41 Davis R, Schonberg J, Rallison J. The lubrication force between two viscous drops.

Physics of Fluids A. 1989;1:77-81.

42 Abid S, Chesters AK. The drainage and rupture of partially-mobile films between colliding drops at constant approach velocity. Int. J. Multiphase Flow. 1994;20:613-629.

43 Ozan SC, Jakobsen HA. On the effect of the approach velocity on the coalescence of fluid particles. Int. J. Multiphase Flow. 2019;119:223-236.

44 Kendoush AA. The virtual mass of a growing and collapsing bubble. AlChE J. 2006;52:2013-2019.

45 Gong SG, Gao NN, Han LC, Luo HA. A theoretical model for bubble coalescence by coupling film drainage with approach processes. Chem. Eng. Sci. 2020;213: 115387.

46 Huang W, Russell RD. Adaptive moving mesh methods. Springer Science & Business Media. 2011.

47 Chesters AK. The modelling of coalescence processes in fluid-liquid dispersions : a review of current understanding. Chem. Eng. Res. Des. 1991;69:259-270.